THE JOURNAL OF PHYSICAL CHEMISTRY LETTERS
A JOURNAL OF THE AMERICAN CHEMICAL SOCIETY

pubs.acs.org/JPCL

Letter

Unbiasing Enhanced Sampling on a High-Dimensional Free Energy Surface with a Deep Generative Model

Yikai Liu, Tushar K. Ghosh, Guang Lin, and Ming Chen*

Cite This: *J. Phys. Chem. Lett.* 2024, 15, 3938−3945

Read Online

ACCESS | Metrics & More | Article Recommendations | Supporting Information

ABSTRACT: Biased enhanced sampling methods that utilize collective variables (CVs) are powerful tools for sampling conformational ensembles. Due to their large intrinsic dimensions, efficiently generating conformational ensembles for complex systems requires enhanced sampling on high-dimensional free energy surfaces. While temperature-accelerated molecular dynamics (TAMD) can trivially adopt many CVs in a simulation, unbiasing the simulation to generate unbiased conformational ensembles requires accurate modeling of a high-dimensional CV probability distribution, which is challenging for traditional density estimation techniques. Here we propose an unbiasing method based on the score-based diffusion model, a deep generative learning method that excels in density estimation across complex data landscapes. We demonstrate that this unbiasing approach, tested on multiple TAMD simulations, significantly outperforms traditional unbiasing methods and can generate accurate unbiased conformational ensembles. With the proposed approach, TAMD can adopt CVs that focus on improving sampling efficiency and the proposed unbiasing method enables accurate evaluation of ensemble averages of important chemical features.

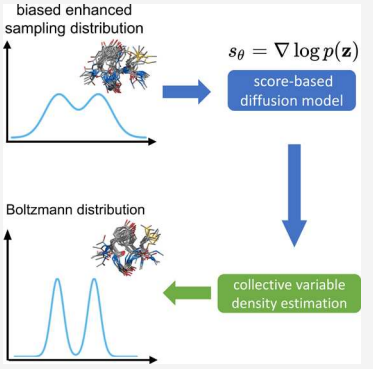

Molecular dynamics (MD) simulations have emerged as a primary computational tool for generating conformational ensembles for studying thermodynamic properties of complex systems in chemistry, biology, and material science.[1] With the assistance of supercomputers,[2,3] it is now possible to perform milliseconds of all-atom MD simulations for medium-sized proteins. To extend MD simulations to broader time and length scales, multiple enhanced sampling methods have been designed to increase the MD sampling efficiency.[4−14] Among all enhanced sampling methods, CV-based enhanced sampling methods focus on several important degrees of freedom that capture systems' essential dynamics. By biasing the probability distribution along CVs, CV-based enhanced sampling methods encourage systems to cross high energy barriers and explore different regions of the energy landscape more efficiently. In general, CV-based enhanced sampling methods focus on converging the free energy surface (FES) associated with the CV. Some CV-based enhanced sampling methods, like metadynamics[5] and umbrella sampling,[15] can generate unbiased conformational ensembles via unbiasing algorithms.

A critical assumption behind CV-based enhanced sampling methods is the manifold hypothesis,[16−18] which posits that high-dimensional all-atom configurations often lie along a low-dimensional latent manifold, and such a low-dimensional manifold can accurately describe the important features of the high-dimensional systems. Traditionally, physics-based CVs are chosen from experimentally measurable properties, geometric descriptors, and order parameters with important underlying physics.[19−21] Recently, machine-learning-based methods that utilize dimensionality reduction techniques have been applied to design CVs.[22−33] Regardless of the CV categories, it is challenging to fully describe a complex system in biochemistry and material science with one or two parameters, a typical number of CVs used in many enhanced sampling simulations. For example, following the two-nearest neighbors method,[34] we estimate the intrinsic dimension (minimum numbers of parameters) for accurately describing amyloid-β 42 ($A\beta_{42}$)[35] to be 7.13, as shown in Figure 1. Fewer than seven CVs will not fully describe this system. Therefore, sampling a high-dimensional FES with more than three CVs are important for exploring conformations of a complex system.[36−39]

There are two challenges associated with studying a high-dimensional FES. First, limited enhanced sampling methods have been developed to sample a high-dimensional FES. For most enhanced sampling methods[38,40−42] that utilize biasing potentials to assist crossing of energy barriers, it is challenging to use many CVs, primarily due to the difficulty of constructing an accurate biasing potential for a high-dimensional FES. Other methods like driven-adiabatic free energy dynamics/temperature-accelerated molecular dynamics (TAMD),[6,7,38,43] which enhance MD sampling by increasing the temperature of certain degrees of freedom, are capable of adopting many CVs in

Received: December 14, 2023
Revised: February 26, 2024
Accepted: March 13, 2024
Published: April 3, 2024

https://doi.org/10.1021/acs.jpclett.3c03515
J. Phys. Chem. Lett. 2024, 15, 3938−3945

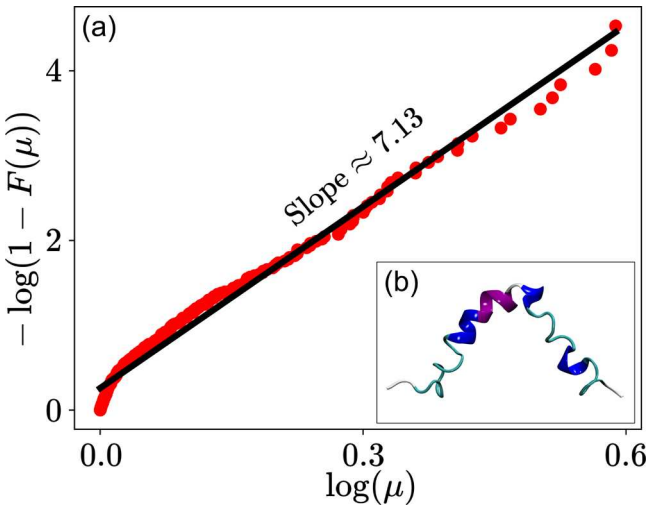

Figure 1. (a) Two-nearest neighbors method that calculates the ratio μ between the nearest and the second nearest neighbor distance for each data point (red dots). $F(\mu)$ is the cumulative distribution of μ. The slope (black fitting line) of $-\log[1-F(\mu)]$ as a function of $\log(\mu)$ is an estimation of the intrinsic dimension of Aβ_{42} (see the Supporting Information for details of the two-nearest neighbors method). (b) Molecular structure of Aβ_{42}.

enhanced sampling simulations, because biasing potential is not required. Second, analyzing and visualizing a high-dimensional FES are nontrivial. One solution is to efficiently generate a conformational ensemble by converging a high-dimensional FES with enhanced sampling. Unbiased conformations can be projected to any features of chemical interest without requiring further sampling, while CVs in enhanced sampling can focus on improving the sampling efficiency. Designing an accurate unbiasing method is needed for this approach.

However, when many CVs are being handled, the task of unbiasing TAMD trajectories to produce unbiased conformational ensembles becomes increasingly complex. This complexity arises from the need for accurate modeling of the high-dimensional, often multimodal, CV probability distribution. Traditional density estimation techniques, such as histogram methods, kernel density estimation (KDE),[44] nearest neighbor density estimation,[45] and the Gaussian mixture model (GMM),[46] often struggle to accurately capture the nuances of such intricate distributions. For instance, KDE suffers in high-dimensional spaces, as it may produce overly smooth or distorted estimates due to the lack of data across the expansive high-dimensional space. On the contrary, the GMM suffers from scalability, initialization sensitivity, and a trivial model selection process. In this paper, we leverage the score-based diffusion model (SBDM)[47] for accurate unbiasing of enhanced sampling simulations with many CVs. A recently popularized denoising diffusion model,[48−50] the SBDM has been successfully used on molecular conformation generation, protein docking, and molecular dynamics.[51−60] In our study, we evaluate the performance of the SBDM-based unbiasing method in TAMD simulations. We will demonstrate that the SBDM is highly effective in accurately estimating CV's probability distributions, outperforming other models in constructing detailed CV probability landscapes. Furthermore, compared to other modern density estimation methods such as normalizing flow, the SBDM can adapt to estimate probability distributions of non-Euclidean CV such as torsion angles, with minor changes to the model architecture.[61] These capacities endow the SBDM-based unbiasing method with superior performance and versatility.

We first introduce the TAMD method and its unbiasing formula. For a system of N particles, we denote its Cartesian coordinates by $\mathbf{r} \equiv (\mathbf{r}_1, \mathbf{r}_2, ..., \mathbf{r}_N)$, and n collective variables by $\mathbf{q} \equiv [q_1(\mathbf{r}), ..., q_n(\mathbf{r})]$. In TAMD, $\mathbf{q}$ are coupled with extended variables $\mathbf{z} \equiv (z_1, ..., z_n)$ with stiff harmonic potentials $\sum_i \kappa_i / 2[q_i(\mathbf{r}) - z_i]^2$. $\mathbf{z}$ typically shares the same topology as $\mathbf{q}$. It has been proven that the free energy surface $A(\mathbf{q})$ can be approximated with the free energy surface of extended variables $A_\kappa(\mathbf{z})$ when $\kappa_i \to \infty$ for all κ_i. TAMD introduces a high temperature $T_h \gg T$ for $\mathbf{z}$ and maintains $\mathbf{r}$ at the desired temperature T. To keep the thermodynamic properties of the system, $\mathbf{z}$ are adiabatically decoupled from $\mathbf{r}$ by assigning each z_i a fictitious mass $\mu_i \gg 1$. With $\beta_h = 1/k_B T_h$, where k_B is the Boltzmann constant, the joint probability distribution of $\mathbf{r}$ and $\mathbf{z}$ from a TAMD simulation satisfies[38]

$$P_{\mathrm{TAMD}}(\mathbf{r}, \mathbf{z}) \approx P_{T_h}(\mathbf{z}) P(\mathbf{r}|\mathbf{z}) \tag{1}$$

where $P_{T_h}(\mathbf{z}) \propto \exp[-\beta_h A_\kappa(\mathbf{z})]$ is the marginal probability distribution of $\mathbf{z}$ and $P(\mathbf{r}|\mathbf{z})$ is the Boltzmann distribution at physical temperature T depending on $\mathbf{z}$. Equation 1 is exact if all $\mu_i \to \infty$. The free energy of collective variables $A_\kappa(\mathbf{z})$ can be easily obtained from TAMD with $A(\mathbf{z}) \approx -k_B T_h \log P_{T_h}(\mathbf{z})$. We are often interested in intuitive features that are different from those of CVs used in an enhanced sampling to understand the properties of the simulated system. Unbiasing enhanced sampling trajectories is necessary to project biased simulation data onto intuitive features. Assuming $\mathbf{Y}(\mathbf{r})$ is a set of low-dimensional intuitive features of interest, the equilibrium probability of $\mathbf{Y}(\mathbf{r}) = \mathbf{y}$ can be written as

$$P(\mathbf{y}) = \int \delta(\mathbf{y} - \mathbf{Y}(\mathbf{r})) \omega(\mathbf{z}) P_{\mathrm{TAMD}}(\mathbf{r}, \mathbf{z})\, \mathrm{d}\mathbf{r}\, \mathrm{d}\mathbf{z} \tag{2}$$

where $\omega(\mathbf{z}) = P_{T_h}(\mathbf{z})^{T_h/T-1}$ is the unbiasing weight.

If $\mathbf{Y}$ can be written as a function of CVs, eq 2 can be reduced to $P(\mathbf{y}) = \int \delta(\mathbf{y} - \mathbf{Y}(\mathbf{z}))\ \omega(\mathbf{z})\ P_{T_h}(\mathbf{z})\ \mathrm{d}\mathbf{z}$. A good estimation of $P_{T_h}(\mathbf{z})$ is crucial for obtaining an accurate $\omega(\mathbf{z})$ in TAMD. Errors in estimating $P_{T_h}(\mathbf{z})$ magnify errors in $\omega(\mathbf{z})$ at a high T_h, leading to an inaccurate $P(\mathbf{y})$. We design a toy problem to demonstrate the importance of accurately modeling $P_{T_h}(\mathbf{z})$ in unbiasing TAMD. In this example, a one-dimensional probability density $P(\mathbf{z})$ at $k_B T = 1$ is constructed with a mixture of Gaussians; the feature of interest $\mathbf{Y}$ is set to be $\mathbf{z}$. The probability is scaled to different T_h values followed by convolution with a Gaussian kernel to obtain a "perturbed" high-temperature probability $\tilde{P}_{T_h}(\mathbf{z})$. $\tilde{P}_{T_h}(\mathbf{z})$ represents an example of inaccurate modeling of $P_{T_h}(\mathbf{z})$. Unbiasing weight $\omega(\mathbf{z})$ is computed from $\tilde{P}_{T_h}(\mathbf{z})$ and used to calculate $P(\mathbf{y})$ with eq 2 (see the Supporting Information for details of the toy problem). Figure 2 demonstrates that the error in $P(y)$ is more sensitive to errors in $\tilde{P}_{T_h}(\mathbf{z})$ when T_h is higher. There are various approaches for constructing $P_{T_h}(\mathbf{z})$. One approach is to use the mean force, such as unified free energy dynamics,[38] the single-sweep method,[62,63] on-the-fly parametrization,[64−67] and reinforced dynamics.[39] However, a large variance of mean force estimator[68] requires enormous samples to control the noise in the mean force, which is highly challenging for converging an FES with more than four CVs. On the contrary, previous studies[36] have shown that $P_{T_h}(\mathbf{z})$ at special

https://doi.org/10.1021/acs.jpclett.3c03515
J. Phys. Chem. Lett. 2024, 15, 3938−3945

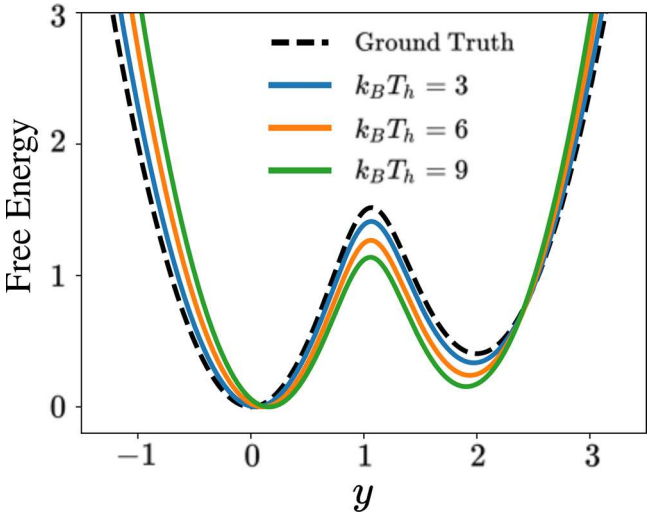

Figure 2. Free energy profiles generated from the unbiasing method of using eq 2 are shown as solid lines with an "inaccurate" estimation of the high-temperature probability. The blue, orange, and green lines correspond to unbiased results from k_BT_h = 3, 6, and 9, respectively, where k_BT = 1 in all three cases. The black dashed line is the ground truth with accurate estimation of the high-temperature probability.

points on a 10-dimensional FES can be evaluated efficiently and accurately by a histogram, which inspires us to use an unsupervised learning method such as the SBDM to model $P_{T_h}(\mathbf{z})$.

We then briefly review the SBDM framework and its usage in density estimation. The SBDM perturbs data distribution to noise prior with a diffusion process over a unit time by a linear stochastic differential equation (SDE):

$$\mathrm{d}\mathbf{z} = f(\mathbf{z}, t)\,\mathrm{d}t + g(t)\,\mathrm{d}\mathbf{w},\ t \in [0, 1] \tag{3}$$

where $f(\mathbf{z}, t)$ and $g(t)$ are user-defined drift and diffusion functions of the SDE, respectively, and $\mathbf{w}$ denotes a standard Wiener process. With a carefully designed SDE, the marginal probability of $\mathbf{z}$ at diffusion time t, $P_t(\mathbf{z})$, changes from data distribution $P_0(\mathbf{z})$ to approximately a simple Gaussian distribution $P_1(\mathbf{z})$. In this paper, we use an SDE with the drift term $f(\mathbf{z}, t) = 0$ and the diffusion function $g(t) = \sqrt{\mathrm{d}\sigma^2(t)/\mathrm{d}t}$, where $\sigma(t)$ represents the noise scale.

For any diffusion process in eq 3, it has a corresponding reverse-time SDE:[69]

$$\mathrm{d}\mathbf{z} = [f(\mathbf{z}, t) - g^2(t)\nabla_{\mathbf{z}} \log P_t(\mathbf{z})]\,\mathrm{d}t + g(t)\,\mathrm{d}\bar{\mathbf{w}} \tag{4}$$

where $\bar{\mathbf{w}}$ is a standard Wiener process in reverse. The trajectories of the reverse SDE have the same marginal densities as those of the forward SDE. Thus, the reverse-time SDE can gradually convert noise into data. The SBDM parametrizes time-dependent score function $\nabla_{\mathbf{z}} \log P_t(\mathbf{z})$ in the reverse SDE with a neural network $\mathbf{s}_{\boldsymbol{\theta}}(\mathbf{z}(t), t)$. To estimate $\nabla_{\mathbf{z}} \log P_t(\mathbf{z})$, a time-dependent score-based model $\mathbf{s}_{\boldsymbol{\theta}}(\mathbf{z}(t), t)$ can be trained via minimizing a denoising score matching loss $J(\theta)$:

$$M(\theta) = \|\mathbf{s}_{\boldsymbol{\theta}}(\mathbf{z}(t), t) - \nabla_{\mathbf{z}(t)} \log P(\mathbf{z}(t)|\mathbf{z}(0))\|_2^2$$
$$J(\theta) = \arg\min_{\boldsymbol{\theta}} \mathbb{E}_t[\lambda(t)\mathbb{E}_{\mathbf{z}(0)}\mathbb{E}_{\mathbf{z}(t)|\mathbf{z}(0)}M(\theta)] \tag{5}$$

with t uniformly sampled in $[0, 1]$, $\lambda(t)$ being a positive weighting function, $\mathbf{z}(0) \sim P_0(\mathbf{z})$, and $\mathbf{z}(t) \sim P(\mathbf{z}(t)|\mathbf{z}(0))$. In our chosen SDE, perturbation kernel $P(\mathbf{z}(t)|\mathbf{z}(0)])$ can be computed in the following closed form:

$$P(\mathbf{z}(t)|\mathbf{z}(0)) = \mathcal{N}(\mathbf{z}(t); \mathbf{z}(0), [\sigma^2(t) - \sigma^2(0)]\mathbf{I}) \tag{6}$$

In our paper, a precomputed weighting function $\lambda(t) = 1/\mathbb{E}\{\|\nabla_{\mathbf{z}(t)} \log P(\mathbf{z}(t)|\mathbf{z}(0))\|_2^2\}$ is used. The score matching loss ensures that the optimal solution to eq 5 equals $\nabla_{\mathbf{z}} \log P_t(\mathbf{z})$ for almost all values of $\mathbf{z}$ and t.

Finally, the SBDM defines a deterministic way to compute data distribution $P_0(\mathbf{z})$ as follows, with $f(\mathbf{z}, t) = 0$:

$$\log P_0(\mathbf{z}) = \log P_1(\mathbf{z}) - \frac{1}{2}\int_0^1 g^2(t)\nabla_{\mathbf{z}}\cdot\mathbf{s}_{\boldsymbol{\theta}}(\mathbf{z}(t), t)\,\mathrm{d}t \tag{7}$$

CVs can be defined as spaces with different topologies. For example, n torsion angles are defined on a hypertorus space $\mathbb{T}^n$, and quaternions that represent rigid-body rotations are defined on a three-dimensional unit sphere $\mathbb{S}^3$. Therefore, extending the SBDM to different topologies is important. In this study, we will focus on the SBDM on a hypertorus space. The theory behind the SBDM holds for compact Riemannian manifolds with subtle modifications. For $\mathbf{z} \in M$, a Riemannian manifold (such as hypertorus $\mathbb{T}^n$), with $\mathbf{w}$ being the Brownian motion on the manifold and $f(\mathbf{z}, t) \in T_{\mathbf{z}}M$, a tangent space, eq 4 still holds.[61] Additionally, due to the compactness of the manifold, the noise prior to $P_1(\mathbf{z})$ becomes a uniform distribution over M. As shown in eq 5, training a denoising score matching model requires sampling from perturbation kernel $P(\mathbf{z}(t)|\mathbf{z}(0))$ of the forward diffusion defined by eq 3. We consider the perturbation kernel on $\mathbb{T}^n$ with a wrapped normal distribution:

$$\mathbf{U}_{\mathbf{d}}(t) = \frac{\|\boldsymbol{z}(0) - \boldsymbol{z}(t) + 2\pi\mathbf{d}\|^2}{2\sigma^2(t)},\ \mathbf{d} \in \mathbb{Z}^n$$
$$P(\mathbf{z}(t)|\mathbf{z}(0)) \propto \sum_{\mathbf{d}} \exp[-\mathbf{U}_{\mathbf{d}}(t)] \tag{8}$$

The rest of the terms in the loss function in eq 5 remain the same. Note that density estimation in eq 7 can be applied to both variables in Euclidean and hypertorus space. The architecture of an SBDM model is highly flexible. For example, an SBDM model can use a residual neural network (ResNet),[70] U-Net,[71] a graph neural network (GNN),[72] etc.

In the following section, we will demonstrate how incorporating SBDM can fulfill the strict density estimation accuracy requirement of unbiasing TAMD, thus allowing TAMD to generate correct unbiased ensembles. We tested the efficiency and accuracy of SBDM to unbiasing TAMD simulations on three systems: (1) alanine dipeptide, (2) glutamine dipeptide, and (3) met-enkephalin (see the Supporting Information for simulation details[34,38,73−92]). In all three systems, we conducted TAMD with torsion angles as collective variables, with a T_h of 1200 K in the first example and a T_h of 900 K in the second and third examples. The physical variables were maintained at 300 K in all three experiments. We then unbiased TAMD with density estimation performed by the SBDM on hypertorus space (see the Supporting Information for details of training SBDM models). In all three experiments, the SBDM is trained with time-dependent score function $\mathbf{s}_{\theta}[\mathbf{z}(t), t]$ parametrized by a U-net architecture. For the diffusion function $g(t) = \sqrt{\mathrm{d}\sigma^2(t)/\mathrm{d}t}$ in the forward SDE of the SBDM, we use $\sigma(t) = \sigma_{\min}{}^{1-t}\sigma_{\max}{}^{t}$, where $\sigma_{\min} = 0.01\pi$ and $\sigma_{\max} = \pi$. Unbiasing TAMD with the SBDM as the density estimation method is

https://doi.org/10.1021/acs.jpclett.3c03515
J. Phys. Chem. Lett. 2024, 15, 3938−3945

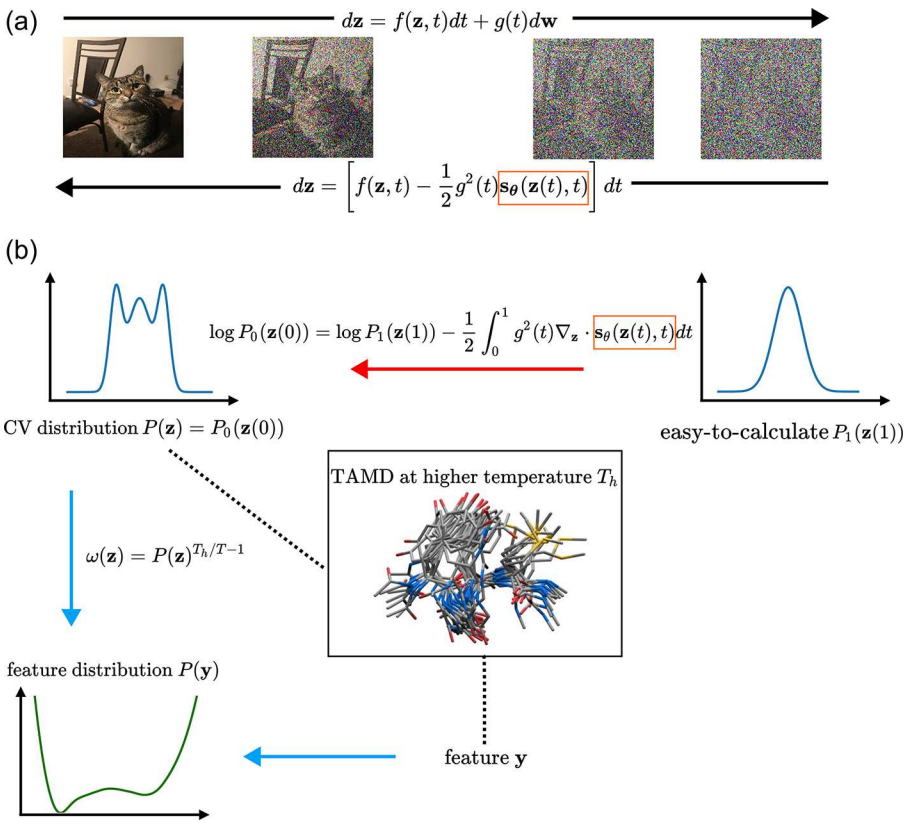

Figure 3. (a) Mechanism of denoising SBDM. During the diffusion process, the data (in this demonstration, a picture) are gradually perturbed to an isotropic Gaussian noise via a forward SDE. (b) Flowchart of unbiasing TAMD with the SBDM. We perform TAMD simulation at a high temperature, T_h, and construct the SBDM for $\mathbf{z}$. The time-dependent score function (boxed in orange) is used to perform the density estimation of the CV, $P(\mathbf{z}) \equiv P_{T_h}(\mathbf{z})$, from a simple distribution, as shown above the red line. Weight $\omega(\mathbf{z})$ of the configurations is evaluated from estimated CV probability $P(\mathbf{z})$. The weight is used to compute the unbiased distribution of features of interest in $P(\mathbf{y})$.

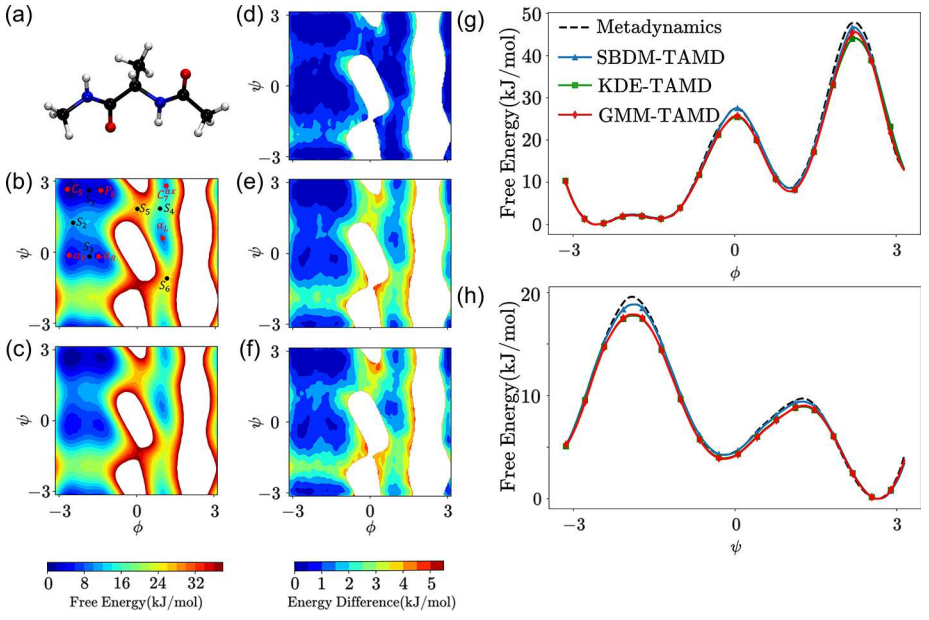

Figure 4. (a) Molecular structure of the alanine dipeptide. FES with respect to backbone dihedral angles of the alanine dipeptide obtained by (b) the WTM and (c) SBDM-TAMD. The red and black points represent the locations of important minima and saddle points on the FES. Absolute free energy differences between the WTM and (d) SBDM-TAMD, (e) KDE-TAMD, and (f) GMM-TAMD. FES of alanine dipeptide with respect to (g) ϕ and (h) ψ.

termed SBDM-TAMD hereafter. The general framework of SBDM-TAMD is summarized in Figure 3. For a fair comparison, we unbiased the same TAMD simulations with kernel density estimation (KDE-TAMD) and a Gaussian mixture model

https://doi.org/10.1021/acs.jpclett.3c03515
J. Phys. Chem. Lett. 2024, 15, 3938−3945

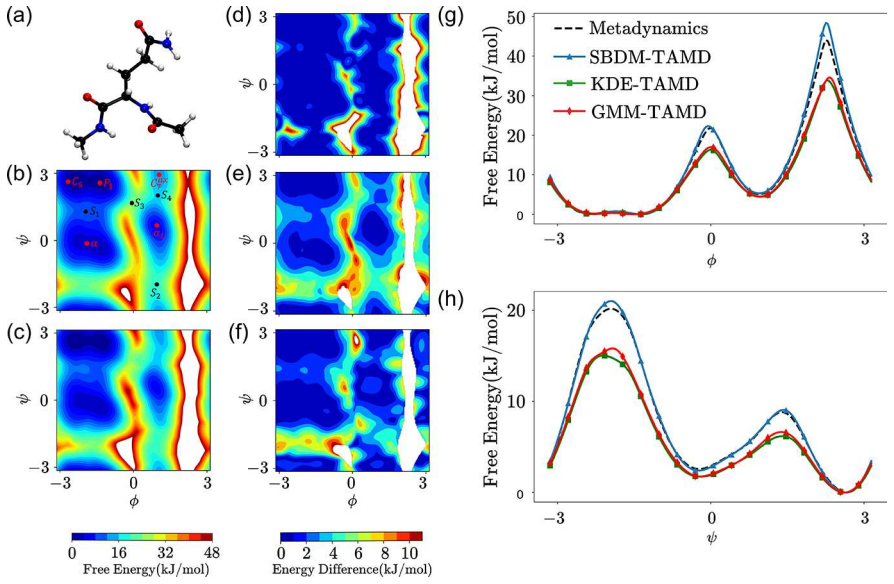

Figure 5. (a) Molecular structure of the glutamine dipeptide. FES of backbone dihedral angles of the glutamine dipeptide calculated by (b) the WTM and (c) SBDM-TAMD. The red and black points represent the locations of important minima and saddle points on the FES. Absolute free energy differences between the WTM and (d) SBDM-TAMD, (e) KDE-TAMD, and (f) GMM-TAMD. FES of the glutamine dipeptide with respect to (g) ϕ and (h) ψ.

(GMM-TAMD) in all three systems, and normalizing flow on hypertorus space (NF-TAMD)[93,94] in the last system. We performed converged well-tempered metadynamics (WTM) simulations at 300 K as the baseline results for all three systems. We will compare the unbiasing results from different density estimation methods to the baseline results. For all examples, multiple WTM simulations, multiple TAMD simulations, and multiple SBDM trainings were performed to ensure reproducibility. Detailed results of all simulations and training results are presented in the Supporting Information.

The first proof-of-concept example is an alanine dipeptide in an aqueous solution with an implicit solvent. This has been a benchmark system with well-established FES in previous studies.[95,96] In both the 500 ns TAMD and the baseline 500 ns WTM, we used Ramachandran angles (ϕ, ψ) as CVs. The accuracy of SBDM-TAMD is demonstrated in Figure 4. The SBDM capably captures the intricate free energy delineated by WTM, as shown in panels c and d of Figure 4. Notably, the model accurately locates all six free energy minima, with the depth of the minima being quantitatively accurate (<1 kJ/mol energy difference). Furthermore, the saddle points, representative of transitions between conformational basins, are also well reproduced. Energy errors in low-free energy saddle points are <2 kJ/mol compared to those of the WTM results. This match implies that the SBDM-TAMD is accurate for studying thermodyanmics of the alanine dipeptide. We notice that for this two-dimensional problem, the KDE and GMM perform relatively well, but still less accurately than the SBDM. Both methods can locate the free energy minima well, but the free energies of saddle points have a larger deviation ($\lesssim$3.5 kJ/mol). The clear disparities in free energy differences, as shown in panels e and f of Figure 4, especially in regions corresponding to the annotated energy minima and saddle points, illustrate the inadequacies of the KDE and GMM for precise FES calculations. The one-dimensional projections shown in panels g and h of Figure 4 also demonstrate the accuracy of SBDM-TAMD.

The second system we studied is the glutamine dipeptide in an aqueous solution with explicit water. A 100 ns TAMD simulation was performed with five dihedral angles on the backbone and the side chain (ϕ, ψ, and χ_1–χ_3) as CVs to enhance the sampling of both backbone and side chain conformations. We also performed a benchmark 100 ns WTM with two backbone dihedral angles as CVs. The result is demonstrated in Figure 5. Projecting an unbiased SBDM-TAMD trajectory onto backbone dihedral angles quantitatively matches the bechmark FES from the WTM. Energy errors of minima on the projected two-dimensional (2D) FES are within 2 kJ/mol, while errors of low-free energy saddles are within 4 kJ/mol. As a comparison, the KDE and GMM both struggle to uphold their precision with increased CV dimensions. Both of these two methods introduce larger errors at S_2 and S_3. This example highlights the SBDM's superior adaptability and accuracy in high-dimensional CVs compared to traditional methods. One-dimensional projections presented in panels g and h of Figure 5 suggest SBDM-TAMD outperforms KDE-TAMD and GMM-TAMD when the free energy is <30 kJ/mol.

The final, more challenging system we studied is the oligopeptide met-enkephalin (Tyr-Gly-Gly-Phe-Met) in an aqueous solution with explicit water, which is a common test case for enhanced sampling techniques.[36,38,97] For 1.0 μs TAMD, we chose 10 backbone dihedral angles (ϕ_1, ψ_1, ..., ϕ_5, and ψ_5) as CVs. The baseline 1.0 μs WTM simulation was performed with a 2D stochastic kinetic embedding (STKE), a manifold learning method that serves as a low-dimensional CV representation that preserves kinetic information.[26] We projected the unbiased SBDM-TAMD trajectory to features like end-to-end distance d_{ee} and a one-dimensional (1D) STKE CV. As a comparison, we unbiased the benchmark WTM simulation[98−100] and projected configurations from the WTM onto the same features. We want to emphasize that generating optimal machine-learning-based CVs for the WTM (STKE in this work) is nontrivial and requires extra simulation data. We compare the unbiased end-to-end distance and 1D STKE, as shown in Figure 6. SBDM-TAMD exhibits high performance, demonstrating a FES that closely aligned with the WTM baseline. The minimum on each projected one-dimensional FES

https://doi.org/10.1021/acs.jpclett.3c03515
J. Phys. Chem. Lett. 2024, 15, 3938−3945

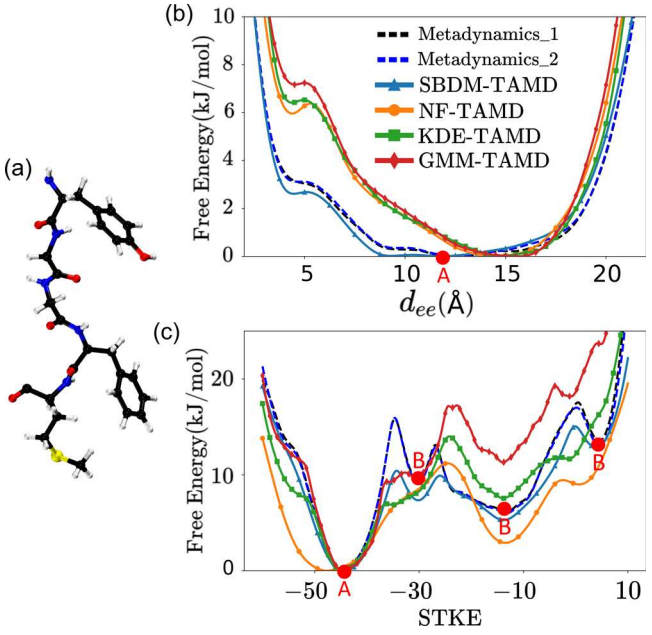

Figure 6. (a) Molecular structure of met-enkephalin. (b and c) FES of the end-to-end distance and 1D STKE, with red dots indicating (A) stable and (B) metastable states.

predicted by SBDM is in good agreement with the benchmark, suggesting SBDM-TAMD is capable of modeling the thermodynamics of a polypeptide. As shown in panel a of Figure 6, SBDM-TAMD predicts that the free energy of d_{ee} values from ∼9.0 to ∼16.0 Å is nearly the same, which is in good agreement with the WTM. However, unbiasing with KDE, GMM, and NF predicts the free energy at a d_{ee} of 10.0 Å is nearly 2 kJ/mol higher than the free free energy at a d_{ee} of 15.0 Å. The KDE, GMM, and NF also underestimate the stability of a metastable conformation with a d_{ee} of 4.0 Å by ∼3 kJ/mol, while SBDM-TAMD agrees well with the WTM. Panel b ofFigure 6 shows that both the WTM and SBDM-TAMD identify all metastable states on 1D STKE with consistent metastability, while the KDE, GMM, and NF fail to predict the correct metastable states and corresponding free energy. Although the FES from SBDM-TAMD slightly underestimates barrier heights, it correctly predicts the location of all barriers. However, unbiasing with the KDE, GMM, and NF results in wrong barrier locations or even missing barriers.

In this work, we developed an unbiasing method based on a score-based diffusion model, a deep generative learning model, to generate unbiased conformational ensembles from collective variable-based biased enhanced sampling simulations. Our method can adapt to simulations with collective variables of large amounts and different topologies. We test the unbiasing method on temperature-accelerated molecular dynamics, an enhanced sampling method that can utilize many collective variables to efficiently explore a high-dimensional free energy surface. Numerical experiments across three systems of 2, 5, and 10 collective variables underscore our unbiasing method's exceptional accuracy and adaptability to high-dimensional collective variables. Although biomolecules were used in the numerical experiments, the developed approach can be used to solve other problems like modeling material phase transitions. Looking ahead, we aim to explore the method's potential in unbiasing simulations with even larger amounts of collective variables and form accurate high-dimensional biasing potentials for wider ranges of enhanced sampling methods.

■ ASSOCIATED CONTENT

Supporting Information

The Supporting Information is available free of charge at https://pubs.acs.org/doi/10.1021/acs.jpclett.3c03515.

Details of MD simulations, reproducing all simulations in this work, SBDM training, two-nearest neighbors intrinsic dimension estimation, and a toy model (PDF)

■ AUTHOR INFORMATION

Corresponding Author

Ming Chen − *Department of Chemistry, Purdue University, West Lafayette, Indiana 47906, United States;* orcid.org/0000-0001-6205-7107; Email: chen4116@purdue.edu

Authors

Yikai Liu − *Department of Mechanical Engineering, Purdue University, West Lafayette, Indiana 47906, United States*

Tushar K. Ghosh − *Department of Chemistry, Purdue University, West Lafayette, Indiana 47906, United States;* orcid.org/0000-0003-4853-0388

Guang Lin − *Department of Mechanical Engineering, Purdue University, West Lafayette, Indiana 47906, United States;* orcid.org/0000-0002-0976-1987

Complete contact information is available at: https://pubs.acs.org/10.1021/acs.jpclett.3c03515

Notes

The authors declare no competing financial interest.

■ ACKNOWLEDGMENTS

T.K.G. and M.C. acknowledge support from the National Science Foundation (EAR-2246687). G.L. and Y.L. gratefully acknowledge the support of the National Science Foundation (DMS-2053746, DMS-2134209, ECCS-2328241, and OAC-2311848) and U.S. Department of Energy (DOE) Office of Science Advanced Scientific Computing Research (DE-SC0023161) and DOE Fusion Energy Science (Grant DE-SC0024583).

■ REFERENCES

(1) Ciccotti, G.; Ferrario, M.; Schuette, C.; et al. Molecular dynamics simulation. *Entropy* **2014**, *16*, 1.

(2) Shaw, D. E.; Grossman, J.; Bank, J. A.; Batson, B.; Butts, J. A.; Chao, J. C.; Deneroff, M. M.; Dror, R. O.; Even, A.; Fenton, C. H. Anton 2: raising the bar for performance and programmability in a special-purpose molecular dynamics supercomputer. *SC '14: Proceedings of the International Conference for High Performance Computing, Networking, Storage and Analysis* **2014**, 41−53.

(3) Shaw, D. E.; Adams, P. J.; Azaria, A.; Bank, J. A.; Batson, B.; Bell, A.; Bergdorf, M.; Bhatt, J.; Butts, J. A.; Correia, T. Anton 3: twenty microseconds of molecular dynamics simulation before lunch. *SC21: International Conference for High Performance Computing, Networking, Storage and Analysis* **2021**, 1−11.

(4) Laio, A.; Parrinello, M. *Escaping free-energy minima* **2002**, *99*, 12562−12566.

(5) Barducci, A.; Bussi, G.; Parrinello, M. Well-tempered metadynamics: a smoothly converging and tunable free-energy method. *Phys. Rev. Lett.* **2008**, *100*, 020603.

(6) Maragliano, L.; Vanden-Eijnden, E. A temperature accelerated method for sampling free energy and determining reaction pathways in rare events simulations. *Chem. Phys. Lett.* **2006**, *426*, 168−175.

(7) Abrams, J. B.; Tuckerman, M. E. Efficient and direct generation of multidimensional free energy surfaces via adiabatic dynamics without coordinate transformations. *J. Phys. Chem. B* **2008**, *112*, 15742−15757.
(8) Darve, E.; Rodríguez-Gómez, D.; Pohorille, A. Adaptive biasing force method for scalar and vector free energy calculations. *J. Chem. Phys.* **2008**, *128*, 144120.
(9) Barducci, A.; Bonomi, M.; Parrinello, M. Metadynamics. *Wiley Interdiscip. Rev. Comput. Mol. Sci.* **2011**, *1*, 826−843.
(10) Abrams, C. F.; Vanden-Eijnden, E. Large-scale conformational sampling of proteins using temperature-accelerated molecular dynamics. *Proc. Natl. Acad. Sci. U.S.A.* **2010**, *107*, 4961−4966.
(11) Yu, T.-Q.; Tuckerman, M. E. Temperature-accelerated method for exploring polymorphism in molecular crystals based on free energy. *Phys. Rev. Lett.* **2011**, *107*, 015701.
(12) Yu, T.-Q.; Chen, P.-Y.; Chen, M.; Samanta, A.; Vanden-Eijnden, E.; Tuckerman, M. Order-parameter-aided temperature-accelerated sampling for the exploration of crystal polymorphism and solid-liquid phase transitions. *J. Chem. Phys.* **2014**, *140*, 214109.
(13) Samanta, A.; Tuckerman, M. E.; Yu, T.-Q.; E, W. Microscopic mechanisms of equilibrium melting of a solid. *Science* **2014**, *346*, 729−732.
(14) Tiwary, P.; Parrinello, M. From metadynamics to dynamics. *Phys. Rev. Lett.* **2013**, *111*, 230602.
(15) Torrie, G.; Valleau, J. Nonphysical sampling distributions in Monte Carlo free-energy estimation: Umbrella sampling. *J. Comput. Phys.* **1977**, *23*, 187−199.
(16) Fefferman, C.; Mitter, S.; Narayanan, H. Testing the manifold hypothesis. *J. Am. Math. Soc.* **2016**, *29*, 983−1049.
(17) Narayanan, H.; Mitter, S. Sample complexity of testing the manifold hypothesis. *NeurIPS Proceedings* **2010**, *23*, 1.
(18) Gorban, A. N.; Tyukin, I. Y. Blessing of dimensionality: mathematical foundations of the statistical physics of data. *Philos. Trans. R. Soc. A: Math. Phys. Eng. Sci.* **2018**, *376*, 20170237.
(19) Hummer, G.; Szabo, A. Free energy reconstruction from nonequilibrium single-molecule pulling experiments. *Proc. Natl. Acad. Sci. U.S.A.* **2001**, *98*, 3658−3661.
(20) Bussi, G.; Gervasio, F. L.; Laio, A.; Parrinello, M. Free-energy landscape for β hairpin folding from combined parallel tempering and metadynamics. *J. Am. Chem. Soc.* **2006**, *128*, 13435−13441.
(21) Granata, D.; Camilloni, C.; Vendruscolo, M.; Laio, A. Characterization of the free-energy landscapes of proteins by NMR-guided metadynamics. *Proc. Natl. Acad. Sci. U.S.A.* **2013**, *110*, 6817−6822.
(22) Das, P.; Moll, M.; Stamati, H.; Kavraki, L. E.; Clementi, C. Low-dimensional, free-energy landscapes of protein-folding reactions by nonlinear dimensionality reduction. *Proc. Natl. Acad. Sci. U.S.A.* **2006**, *103*, 9885−9890.
(23) Ferguson, A. L.; Panagiotopoulos, A. Z.; Debenedetti, P. G.; Kevrekidis, I. G. Integrating diffusion maps with umbrella sampling: Application to alanine dipeptide. *J. Chem. Phys.* **2011**, *134*, 135103.
(24) Rohrdanz, M. A.; Zheng, W.; Maggioni, M.; Clementi, C. Determination of reaction coordinates via locally scaled diffusion map. *J. Chem. Phys.* **2011**, *134*, 124116.
(25) Noé, F.; Clementi, C. Kinetic distance and kinetic maps from molecular dynamics simulation. *J. Chem. Theory Comput* **2015**, *11*, 5002−5011.
(26) Zhang, J.; Chen, M. Unfolding hidden barriers by active enhanced sampling. *Phys. Rev. Lett.* **2018**, *121*, 010601.
(27) Fu, X.; Xie, T.; Rebello, N. J.; Olsen, B. D.; Jaakkola, T. Simulate time-integrated coarse-grained molecular dynamics with geometric machine learning. *ICLR Workshop Deep Generative Models High Structural Data*; 2022.
(28) Ceriotti, M.; Tribello, G. A.; Parrinello, M. *Proc. Natl. Acad. Sci. U.S.A* **2011**, *108*, 13023−13028.
(29) Tiwary, P.; Berne, B. Spectral gap optimization of order parameters for sampling complex molecular systems. *Proc. Natl. Acad. Sci. U.S.A.* **2016**, *113*, 2839−2844.
(30) Mendels, D.; Piccini, G.; Parrinello, M. Collective variables from local fluctuations. *J. Phys. Chem. Lett.* **2018**, *9*, 2776−2781.
(31) Ribeiro, J. M. L.; Bravo, P.; Wang, Y.; Tiwary, P. Reweighted autoencoded variational Bayes for enhanced sampling (RAVE). *J. Chem. Phys.* **2018**, *149*, 072301.
(32) Wang, Y.; Ribeiro, J. M. L.; Tiwary, P. Past-future information bottleneck for sampling molecular reaction coordinate simultaneously with thermodynamics and kinetics. *Nat. Commun.* **2019**, *10*, 3573.
(33) Nuske, F.; Keller, B. G.; Pérez-Hernández, G.; Mey, A. S.; Noé, F. Variational approach to molecular kinetics. *J. Chem. Theory Comput* **2014**, *10*, 1739−1752.
(34) Facco, E.; d'Errico, M.; Rodriguez, A.; Laio, A. Estimating the intrinsic dimension of datasets by a minimal neighborhood information. *Sci. Rep.* **2017**, *7*, 12140.
(35) Findeis, M. A. The role of amyloid β peptide 42 in Alzheimer's disease. *Pharmacol. Ther.* **2007**, *116*, 266−286.
(36) Chen, M.; Yu, T.-Q.; Tuckerman, M. E. Locating landmarks on high-dimensional free energy surfaces. *Proc. Natl. Acad. Sci. U.S.A.* **2015**, *112*, 3235−3240.
(37) Yu, T.-Q.; Chen, P.-Y.; Chen, M.; Samanta, A.; Vanden-Eijnden, E.; Tuckerman, M. Order-parameter-aided temperature-accelerated sampling for the exploration of crystal polymorphism and solid-liquid phase transitions. *J. Chem. Phys.* **2014**, *140*, 214109.
(38) Chen, M.; Cuendet, M. A.; Tuckerman, M. E. Heating and flooding: A unified approach for rapid generation of free energy surfaces. *J. Chem. Phys.* **2012**, *137*, 024102.
(39) Zhang, L.; Wang, H.; E, W. Reinforced dynamics for enhanced sampling in large atomic and molecular systems. *J. Chem. Phys.* **2018**, *148*, 124113.
(40) Debnath, J.; Parrinello, M. Gaussian Mixture-Based Enhanced Sampling for Statics and Dynamics. *J. Phys. Chem. Lett.* **2020**, *11*, 5076−5080.
(41) Zhang, L.; Wang, H.; E, W. Reinforced dynamics for enhanced sampling in large atomic and molecular systems. *J. Chem. Phys.* **2018**, *148*, 124113.
(42) Zhang, J.; Lei, Y.-K.; Yang, Y. I.; Gao, Y. Q. Deep learning for variational multiscale molecular modeling. *J. Chem. Phys.* **2020**, *153*, 174115.
(43) Cuendet, M. A.; Tuckerman, M. E. Free energy reconstruction from metadynamics or adiabatic free energy dynamics simulations. *J. Chem. Theory Comput* **2014**, *10*, 2975−2986.
(44) Chen, Y.-C. A tutorial on kernel density estimation and recent advances. *Biostat. Epidemiol.* **2017**, *1*, 161−187.
(45) Mack, Y.; Rosenblatt, M. Multivariate k-nearest neighbor density estimates. *J. Multivar. Anal.* **1979**, *9*, 1−15.
(46) Reynolds, D. A. Gaussian mixture models. *Encyclopedia of Biometrics* **2009**, *741*, 659.
(47) Song, Y.; Sohl-Dickstein, J.; Kingma, D. P.; Kumar, A.; Ermon, S.; Poole, B. Score-Based Generative Modeling through Stochastic. *arXiv* **2021**, DOI: 10.48550/arXiv.2011.13456.
(48) Ho, J.; Jain, A.; Abbeel, P. Denoising diffusion probabilistic models. *NeurIPS Proceedings* **2020**, *33*, 6840−6851.
(49) De Bortoli, V.; Thornton, J.; Heng, J.; Doucet, A. Diffusion Schrödinger bridge with applications to score-based generative modeling. *NeurIPS Proceedings* **2021**, *34*, 17695−17709.
(50) Kingma, D.; Salimans, T.; Poole, B.; Ho, J. Variational diffusion models. *NeurIPS Proceedings* **2021**, *34*, 21696−21707.
(51) Xu, M.; Yu, L.; Song, Y.; Shi, C.; Ermon, S.; Tang, J. Geodiff: A geometric diffusion model for molecular conformation generation. *ICLR*; 2022.
(52) Jo, J.; Lee, S.; Hwang, S. J. Score-based generative modeling of graphs via the system of stochastic differential equations. *arXiv* **2022**, DOI: 10.48550/arXiv.2202.02514.
(53) Lee, J. S.; Kim, J.; Kim, P. M. Score-based generative modeling for de novo protein design. *Nat. Comput. Sci.* **2023**, *3*, 382−392.
(54) Huang, L.; Zhang, H.; Xu, T.; Wong, K.-C. Mdm: Molecular diffusion model for 3d molecule generation. *AAAI* **2023**, *37*, 5105−5112.
(55) Jing, B.; Corso, G.; Chang, J.; Barzilay, R.; Jaakkola, T. Torsional diffusion for molecular conformer generation. *NeurIPS Proceedings* **2022**, *35*, 24240−24253.

(56) Corso, G.; Stärk, H.; Jing, B.; Barzilay, R.; Jaakkola, T. Diffdock: Diffusion steps, twists, and turns for molecular docking. *ICLR*; 2023.
(57) Arts, M.; Garcia Satorras, V.; Huang, C.-W.; Zugner, D.; Federici, M.; Clementi, C.; Noé, F.; Pinsler, R.; van den Berg, R. Two for one: Diffusion models and force fields for coarse-grained molecular dynamics. *J. Chem. Theory Comput* **2023**, *19*, 6151−6159.
(58) Wu, F.; Li, S. Z. DIFFMD: a geometric diffusion model for molecular dynamics simulations. *AAAI'23/IAAI'23/EAAI'23: Proceedings of the Thirty-Seventh AAAI Conference on Artificial Intelligence and Thirty-Fifth Conference on Innovative Applications of Artificial Intelligence and Thirteenth Symposium on Educational Advances in Artificial Intelligence* **2023**, *37*, 5321−5329.
(59) Lee, S.; Jo, J.; Hwang, S. J. Exploring chemical space with score-based out-of-distribution generation. *Proceedings of the 40 th International Conference on Machine Learning* **2023**, 18872−18892.
(60) Wang, Y.; Herron, L.; Tiwary, P. From data to noise to data for mixing physics across temperatures with generative artificial intelligence. *Proc. Natl. Acad. Sci. U. S. A.* **2022**, *119*, e2203656119.
(61) De Bortoli, V.; Mathieu, E.; Hutchinson, M.; Thornton, J.; Teh, Y. W.; Doucet, A. Riemannian score-based generative modelling. *NeurIPS Proceedings* **2022**, *35*, 2406−2422.
(62) Maragliano, L.; Vanden-Eijnden, E. Single-sweep methods for free energy calculations. *J. Chem. Phys.* **2008**, *128*, 184110.
(63) Monteferrante, M.; Bonella, S.; Meloni, S.; Ciccotti, G. Modified single sweep method for reconstructing free-energy landscapes. *Mol. Simul.* **2009**, *35*, 1116−1129.
(64) Abrams, C. F.; Vanden-Eijnden, E. On-the-fly free energy parameterization via temperature accelerated molecular dynamics. *Chem. Phys. Lett.* **2012**, *547*, 114−119.
(65) Paz, S. A.; Abrams, C. F. Free Energy and Hidden Barriers of the β-Sheet Structure of Prion Protein. *J. Chem. Theory Comput* **2015**, *11*, 5024−5034.
(66) Paz, S. A.; Vanden-Eijnden, E.; Abrams, C. F. Polymorphism at 129 dictates metastable conformations of the human prion protein N-terminal ß-sheet. *Chem. Sci.* **2017**, *8*, 1225−1232.
(67) Paz, S. A.; Maragliano, L.; Abrams, C. F. Effect of Intercalated Water on Potassium Ion Transport through Kv1.2 Channels Studied via On-the-Fly Free-Energy Parametrization. *J. Chem. Theory Comput* **2018**, *14*, 2743−2750.
(68) Samanta, A.; Chen, M.; Yu, T.-Q.; Tuckerman, M.; E, W. Sampling saddle points on a free energy surface. *J. Chem. Phys.* **2014**, *140*, 164109.
(69) Anderson, B. D. Reverse-time diffusion equation models. *Stoch. Process. Their Appl.* **1982**, *12*, 313−326.
(70) He, K.; Zhang, X.; Ren, S.; Sun, J. Deep residual learning for image recognition. *2016 IEEE Conference on Computer Vision and Pattern Recognition (CVPR)* **2016**, 770−778.
(71) Ronneberger, O.; Fischer, P.; Brox, T. U-Net: Convolutional Networks for Biomedical Image Segmentation. *Medical Image Computing and Computer-Assisted Intervention − MICCAI 2015* **2015**, *9351*, 234−241.
(72) Scarselli, F.; Gori, M.; Tsoi, A. C.; Hagenbuchner, M.; Monfardini, G. The graph neural network model. *IEEE Transactions on Neural Networks* **2009**, *20*, 61−80.
(73) Berendsen, H.; van der Spoel, D.; van Drunen, R. GROMACS: A message-passing parallel molecular dynamics implementation. *Comput. Phys. Commun.* **1995**, *91*, 43−56.
(74) Lindahl, E.; Hess, B.; Van Der Spoel, D. GROMACS 3.0: a package for molecular simulation and trajectory analysis. *Mol. Model. Annu.* **2001**, *7*, 306−317.
(75) Van Der Spoel, D.; Lindahl, E.; Hess, B.; Groenhof, G.; Mark, A. E.; Berendsen, H. J. C. GROMACS: Fast, flexible, and free. *J. Comput. Chem.* **2005**, *26*, 1701−1718.
(76) Hess, B.; Kutzner, C.; van der Spoel, D.; Lindahl, E. GROMACS 4: Algorithms for Highly Efficient, Load-Balanced, and Scalable Molecular Simulation. *J. Chem. Theory Comput* **2008**, *4*, 435−447.
(77) Pronk, S.; Páll, S.; Schulz, R.; Larsson, P.; Bjelkmar, P.; Apostolov, R.; Shirts, M. R.; Smith, J. C.; Kasson, P. M.; van der Spoel, D.; et al. GROMACS 4.5: a high-throughput and highly parallel open source molecular simulation toolkit. *Bioinformatics* **2013**, *29*, 845−854.
(78) Lindorff-Larsen, K.; Piana, S.; Palmo, K.; Maragakis, P.; Klepeis, J. L.; Dror, R. O.; Shaw, D. E. Improved side-chain torsion potentials for the Amber ff99SB protein force field. *Proteins: Struct., Funct., Bioinform.* **2010**, *78*, 1950−1958.
(79) Bussi, G.; Donadio, D.; Parrinello, M. Canonical sampling through velocity rescaling. *J. Chem. Phys.* **2007**, *126*, 014101.
(80) Jorgensen, W. L.; Chandrasekhar, J.; Madura, J. D.; Impey, R. W.; Klein, M. L. Comparison of simple potential functions for simulating liquid water. *J. Chem. Phys.* **1983**, *79*, 926−935.
(81) Darden, T.; York, D.; Pedersen, L. Particle mesh Ewald: An N log (N) method for Ewald sums in large systems. *J. Chem. Phys.* **1993**, *98*, 10089−10092.
(82) Essmann, U.; Perera, L.; Berkowitz, M. L.; Darden, T.; Lee, H.; Pedersen, L. G. A smooth particle mesh Ewald method. *J. Chem. Phys.* **1995**, *103*, 8577−8593.
(83) Hess, B. P. P-LINCS: A Parallel Linear Constraint Solver for Molecular Simulation. *J. Chem. Theory Comput* **2008**, *4*, 116−122.
(84) Bonomi, M.; Branduardi, D.; Bussi, G.; Camilloni, C.; Provasi, D.; Raiteri, P.; Donadio, D.; Marinelli, F.; Pietrucci, F.; Broglia, R. A.; et al. PLUMED: A portable plugin for free-energy calculations with molecular dynamics. *Comput. Phys. Commun.* **2009**, *180*, 1961−1972.
(85) Tribello, G. A.; Bonomi, M.; Branduardi, D.; Camilloni, C.; Bussi, G. PLUMED 2: New feathers for an old bird. *Comput. Phys. Commun.* **2014**, *185*, 604−613.
(86) Bonomi, M.; Bussi, G.; Camilloni, C.; Tribello, G. A.; Banáš, P.; Barducci, A.; Bernetti, M.; Bolhuis, P. G.; Bottaro, S.; Branduardi, D.; et al. Promoting transparency and reproducibility in enhanced molecular simulations. *Nat. Methods* **2019**, *16*, 670−673.
(87) Barducci, A.; Bussi, G.; Parrinello, M. Well-tempered metadynamics: a smoothly converging and tunable free-energy method. *Phys. Rev. Lett.* **2008**, *100*, 020603.
(88) Zhang, J.; Chen, M. Unfolding Hidden Barriers by Active Enhanced Sampling. *Phys. Rev. Lett.* **2018**, *121*, 010601.
(89) Tancik, M.; Srinivasan, P.; Mildenhall, B.; Fridovich-Keil, S.; Raghavan, N.; Singhal, U.; Ramamoorthi, R.; Barron, J.; Ng, R. Fourier features let networks learn high frequency functions in low dimensional domains. *NeurIPS Proceedings* **2020**, *33*, 7537−7547.
(90) Wu, Y.; He, K. *Group normalization.* **2018**, *11217*, 3−19.
(91) Chen, R. T.; Rubanova, Y.; Bettencourt, J.; Duvenaud, D. K. Neural ordinary differential equations. *NeurIPS Proceedings* **2018**, *31*, 1.
(92) Tiwary, P.; Parrinello, M. A Time-Independent Free Energy Estimator for Metadynamics. *J. Phys. Chem. B* **2015**, *119*, 736−742.
(93) Rezende, D. J.; Papamakarios, G.; Racaniere, S.; Albergo, M.; Kanwar, G.; Shanahan, P.; Cranmer, K. Normalizing flows on tori and spheres. *Proceedings of the 37 th International Conference on Machine Learning* **2020**, 8083−8092.
(94) Köhler, J.; Krämer, A.; Noé, F. Smooth normalizing flows. *NeurIPS Proceedings* **2021**, *34*, 2796−2809.
(95) Strodel, B.; Wales, D. J. Free energy surfaces from an extended harmonic superposition approach and kinetics for alanine dipeptide. *Chem. Phys. Lett.* **2008**, *466*, 105−115.
(96) Smith, P. E. The alanine dipeptide free energy surface in solution. *J. Chem. Phys.* **1999**, *111*, 5568−5579.
(97) Hénin, J.; Fiorin, G.; Chipot, C.; Klein, M. L. Exploring Multidimensional Free Energy Landscapes Using Time-Dependent Biases on Collective Variables. *J. Chem. Theory Comput* **2010**, *6*, 35−47.
(98) Sutto, L.; D'Abramo, M.; Gervasio, F. L. Comparing the efficiency of biased and unbiased molecular dynamics in reconstructing the free energy landscape of met-enkephalin. *J. Chem. Theory Comput* **2010**, *6*, 3640−3646.
(99) Sutto, L.; Marsili, S.; Gervasio, F. L. New advances in metadynamics. *Wiley Interdisciplinary Reviews: Computational Molecular Science* **2012**, *2*, 771−779.
(100) Sicard, F.; Senet, P. Reconstructing the free-energy landscape of Met-enkephalin using dihedral principal component analysis and well-tempered metadynamics. *J. Chem. Phys.* **2013**, *138*, 235101.

https://doi.org/10.1021/acs.jpclett.3c03515
J. Phys. Chem. Lett. 2024, 15, 3938−3945